Journal of Fluids and Structures 125 (2024) 104049

Contents lists available at ScienceDirect

Journal of Fluids and Structures

journal homepage: www.elsevier.com/locate/jfs

Numerical modelling of a vertical cylinder with dynamic response in steep and breaking waves using smoothed particle hydrodynamics

Yong Yang [a,*], Aaron English [b], Benedict D. Rogers [a], Peter K. Stansby [a], Dimitris Stagonas [c], Eugeny Buldakov [d], Samuel Draycott [a]

[a] School of Engineering, University of Manchester, Oxford Road, Manchester M13 9PL, United Kingdom
[b] Department of Engineering and Architecture, University of Parma, Parco Area delle Scienze 181/A, 43124 Parma, Italy
[c] Department of Civil and Environmental Engineering, University of Cyprus, 1 Panepistimiou Avenue, P.O. Box 20537, 1678 Nicosia, Cyprus
[d] Department of Civil, Environmental and Geomatic Engineering, University College London, Gower Street, London WC1E 6BT, United Kingdom

ARTICLE INFO

Keywords:
Fluid–structure interaction
Near-breaking and spilling breaking waves
Dynamic response
Open boundary conditions
Smoothed particle hydrodynamics
DualSPHysics

ABSTRACT

Highly nonlinear near-breaking and spilling breaking wave groups are common extreme events in the ocean. Accurate force prediction on offshore and ocean structures in these extreme wave conditions based on numerical approaches remains a problem of great practical importance. Most previous numerical studies have concentrated on non-breaking wave forces on rigid structures. Taking advantage of the smoothed particle hydrodynamics (SPH) method, this paper addresses this problem and presents the development and validation of a numerical model for highly nonlinear hydrodynamics of near-breaking and spilling breaking waves interacting with a vertical cylindrical structure using the SPH-based DualSPHysics solver. Open boundaries are applied for the generation of extreme wave conditions. The free-surface elevation and flow kinematics pre-computed within another numerical model are used as boundary conditions at the inlet of a smaller 3-D SPH-based numerical model to replicate the near-breaking and spilling breaking waves generated in a physical wave flume. A damping zone used for wave absorption is arranged at the end of the domain before the outlet. Numerical results are validated against experimental measurements of surface elevation and horizontal force on the vertical cylinder, demonstrating an agreement. After validation using a fixed model for the cylinder, a dynamic model is used to study the response to extreme wave events. Numerical results have also shown that the spilling breaking wave forces are significantly larger compared with near-breaking wave forces, and the secondary load cycle phenomenon becomes larger with dynamic response included in the present study.

1. Introduction

Prediction of the wave loading on structures has long been an important topic in marine and ocean engineering and is now of great interest in the development of offshore renewable energy. Wave forces due to non-breaking waves have been extensively investigated. However, marine vessels, offshore systems and ocean platforms are subject to violent hydrodynamics including near-breaking and spilling breaking waves which are common events in extreme sea conditions. Investigations of replicating these extreme conditions

* Corresponding author.
E-mail address: yong.yang-3@postgrad.manchester.ac.uk (Y. Yang).

https://doi.org/10.1016/j.jfluidstructs.2023.104049
Received 19 September 2023; Received in revised form 27 November 2023; Accepted 11 December 2023
Available online 20 January 2024

and associated loading on structures through laboratory experiments in a physical flume (e.g., Zang et al., 2010; Chen et al., 2018; Esandi et al., 2020) are of great importance for engineering design. The development of a reliable numerical flume as an effective tool to address this problem will be the main task of the present study. Numerical models are more efficient for the study involving a range of test cases compared with laboratory experiments and are complementary to experiments.

Experiments provide an effective approach for problems associated with the wave loading on offshore and ocean structures in various extreme wave conditions and can be used for the validation of numerical models. Experimental investigations of interaction of steep and breaking regular waves (e.g., Wang et al., 2020; Li et al., 2022; Zhu et al., 2022; Gao et al., 2023) and irregular waves (e.g., Ji et al., 2015; Suja-Thauvin et al., 2017; Zhu et al., 2022) with offshore and ocean structures were presented in literature with different aims and findings. Loads on a jacket structure in steep and breaking regular waves were investigated experimentally in Wang et al. (2020). It was shown that an impulsive slamming force component occurred in the breaking waves compared with steep non-breaking waves brings significant uncertainty. Li et al. (2022) investigated the wave force on a circular cylinder due to steep regular waves in experiments, where it was found that the secondary load cycle (appears as a rapid variation after the peak force in wave force time history) highly depends on the wave steepness with proposing a critical curve $kA = 0.3\tanh(kh)$ (k is wavenumber, A is wave crest height and h is water depth) to predict the occurrence of secondary load cycle. Breaking regular waves slamming on an offshore wind jacket structure was investigated experimentally in Gao et al. (2023), where the effect of the relative location between the structure and wave breaker position on the slamming force was studied. An experimental study of the interaction of irregular waves with a bottom-mounted larger vertical cylinder was presented in Ji et al. (2015), where it was concluded that the wave forces increase as the wave steepness increases. Experimental investigation of a monopile in steep and breaking irregular wave conditions was presented in Suja-Thauvin et al. (2017). Two physical models were tested whereby one was flexible (1st and 2nd eigenfrequencies and 1st mode shape are representative of those of a full-scale 4 MW wind turbine) whilst the other one was stiff. It was found that the phenomenon of secondary load cycle is not directly linked to ringing responses of the structure and a secondary load cycle is not shown in some events with a strong ringing response. Both breaking regular and irregular wave slamming forces on a monopile were investigated experimentally in Zhu et al. (2022), where it was found that the wave slamming process involves high nonlinearity and energy dissipation for extreme irregular wave conditions.

Extreme wave conditions using regular waves and irregular waves are presented in a large number of experimental investigations. However, focused waves are suggested as representative for reproducing statistically representative extreme conditions to investigate extreme wave forces on offshore and ocean structures in short time frames. Different wave generation approaches are developed to achieve the focusing of waves at a particular point in space and time, including the dispersive focusing method based on linear theory (Rapp and Melville, 1990), the iterative focusing method correcting initial phases (Chaplin, 1996), and the iterative focusing method correcting both initial phases and amplitudes (Schmittner et al., 2009; Fernández et al., 2014; Draycott et al., 2019). An improved iterative wave focusing methodology considering a linearised amplitude spectrum instead of a full nonlinear spectrum to correct initial phases and amplitudes was presented in Buldakov et al. (2017). The experimental investigation of wave forces on a vertical cylinder due to near-breaking and spilling breaking focused waves with controlled generation using this improved iterative wave focusing methodology was presented in Esandi et al. (2020). It was concluded that forces acting on the cylinder due to spilling breaking waves are significantly larger than forces due to highly nonlinear non-breaking waves. The numerical model developed in the presented study is validated with the measurements in this experimental study.

Experimental investigations of the interaction of steep, near-breaking and breaking waves with offshore and ocean structures reveal the significantly larger breaking wave forces compared with non-breaking wave forces, the secondary load cycle formation in highly nonlinear fluid–structure interaction and the high nonlinearity involved in the slamming process. Meanwhile, offshore structures designed for a standard storm more commonly experience focused or nearly focused symmetrical waves with spilling breaking in a moderately severe sea state (Esandi et al., 2020). Therefore, for the development of a reliable numerical model, the model's ability at capturing these phenomena within the physical process of interaction of near-breaking and spilling breaking waves with the structure is of great importance and should be validated. This is the main aim of this paper. The second aim is to consider a dynamic model (with the small-amplitude oscillations due to stiffness at the hinge, and the cylinder itself is rigid for both the fixed model and the dynamic model in the present study) for the cylinder to extend the numerical model's ability to study the dynamic response to near-breaking and spilling breaking waves.

Typical methods for prediction of hydrodynamic loads due to the incident waves and currents or combined wave–current conditions are the Morison equation (Morison et al., 1950), potential flow theory (e.g., Faltinsen, 1993), hybrid approaches using the Morison equation and potential flow theory, and computational fluid dynamics (CFD) as concluded in Subbulakshmi et al. (2022). However, the Morison equation is applicable for slender objects with a small characteristic dimension and accounts for the viscous effects while potential flow theory is applicable for larger structures with the characteristic dimension significantly larger than the wavelength (characteristic dimension/wavelength > 0.2) and accounts for the diffraction and radiation effects. Though the hybrid approach of the Morison equation and potential flow theory is widely used in engineering, it still suffers from difficulties in problems involving extreme wave conditions, especially breaking waves. Mesh-based CFD methods are mature and have dominated the field of CFD. However, difficulties exist in solving problems with a free surface, moving interface, deformable boundary and highly nonlinear deformation of the fluid body (Liu and Liu, 2010; Ye et al., 2019; Luo et al., 2021). Meanwhile, these mesh-based CFD solvers are normally based on the Eulerian algorithm and special treatments such as Volume-of-Fluid (VOF) and Level Set (LS) are required to track the free surface.

Smoothed particle hydrodynamics (SPH) (Gingold and Monaghan, 1977; Lucy, 1977) as a Lagrangian and meshless technique for CFD has received increasing attention, which was initially applied for numerical modelling of free-surface flows in Monaghan (1994). Highly violent and nonlinear flows are involved in the present study for simulating interaction of near-breaking and spilling breaking

waves interacting with the cylinder. SPH is ideally suited to fluid problems with large deformation and high nonlinearity (e.g., Dalrymple and Rogers, 2006; Gómez-Gesteira et al., 2010; Sun et al., 2015; Lind et al., 2016; Chow et al., 2019; Domínguez et al., 2019) due to its meshless and Lagrangian characteristics that there is no mesh connection between particles which makes it independent of mesh distortion. As the motion of the fluid is represented by the motion of the particles, the SPH method is allowed to detect the free surface in free-surface flows and the interface in multi-phase flows without any of the special treatments required in mesh-based CFD methods. Therefore, simulating violent free-surface flows including breaking waves based on the SPH method has advantages in several aspects compared with using other numerical methods, such as automatic free-surface simulation and avoiding issues with mesh generation.

The SPH method can be categorised into two groups of the traditional weakly compressible SPH (WCSPH) and the incompressible SPH (ISPH). In WCSPH, the fluids are considered as weakly compressible with the use of an equation of state to relate the pressure to the density (Monaghan, 1994). In ISPH, the fluids remain incompressible with the pressure obtained by solving the pressure Poisson equation (Shao and Lo, 2003). WCSPH is an explicit time-stepping method with physical quantities of particles updated at each time step whilst ISPH is a semi-implicit method that requires the solution of a matrix equation at each time step (Lee et al., 2008; Hughes and Graham, 2010). Numerical modelling of spilling and plunging breaking waves without a structure is a popular topic based on WCSPH and ISPH. Plunging breaking waves were simulated based on WCSPH (Dalrymple and Rogers, 2006; Issa and Violeau, 2009; Makris et al., 2016) with a focus on the breaking processes while both spilling and plunging breaking waves were investigated based on WCSPH in De Padova et al. (2020). Using ISPH, spilling and plunging breaking waves were simulated with a focus on coupling a turbulence model with the ISPH model (Shao, 2006) and improving the ISPH model for free-surface tracking (Khayyer et al., 2008). Compared with plunging breaking waves which are unusual in deep water areas, spilling breaking waves are more common in extreme sea conditions (Esandi et al., 2020). However, to the authors' knowledge there are few previous investigations with validations against experiments for the prediction of wave forces on offshore and ocean structures due to spilling breaking waves interacting with a structure based on SPH. Two studies (Lind et al., 2016; Chow et al., 2019) using ISPH compared the wave forces on a vertical cylinder due to breaking waves generated using focused waves with the experimental measurements provided in Zang et al. (2010). Lind et al. (2016) investigated the wave forces on a vertical cylinder due to plunging breaking waves and spilling breaking waves in 2-D using ISPH with a Froude–Krylov approximation for the prediction of 3-D wave forces. Chow et al. (2019) developed a 3-D numerical wave basin based on ISPH and investigated the wave forces on a vertical cylinder due to plunging breaking waves. Wen et al. (2016) investigated regular waves interacting with a vertical cylinder using WCSPH and compared this with linear diffraction theory, where it was shown that the influence of nonlinear effects on wave force prediction increases in waves with larger wave amplitudes and the WCSPH model is required for steeper waves since the linear approach fails. Recently, some new treatments for the WCSPH model have been presented. A new correction is introduced to the density diffusion term in the continuity equation with the correction of pressure errors at the boundary (Fourtakas et al., 2019). The dynamic boundary condition has been improved to avoid the gap commonly observed between the fluid and the solid boundary (English et al., 2022). In addition, the Velocity-divergence Error Mitigating (VEM) and Volume Conservation Shifting (VCS) schemes (Khayyer et al., 2023) and an acoustic damper term (Sun et al., 2023) give more options to reduce the unphysical noise.

The solver used in the present study is the WCSPH-based DualSPHysics which is an open-source SPH code (Domínguez et al., 2022). DualSPHysics has shown to be robust and accurate for simulating free-surface flows including waves (e.g., Altomare et al., 2015, 2017; Zhang et al., 2018; Verbrugghe et al., 2019) and currents (e.g., Tafuni et al., 2018), wave–current interaction (e.g., Yang et al., 2023a), and fluid–structure interaction (e.g., Tagliafierro et al., 2022; Tan et al., 2023; Capasso et al., 2023; Yang et al., 2023b; Tagliafierro et al., 2023). The prediction of wave forces on a vertical cylinder due to near-breaking and spilling breaking waves based on SPH is the main purpose in the present study. Several typical methods are available to generate waves within DualSPHysics. A numerical wave flume using a piston-type or flap-type wavemaker for wave generation and a damping zone for wave absorption (e.g., Altomare et al., 2017; Zhang et al., 2018) is well tested within DualSPHsyics. Instead of using a wavemaker, open boundaries (Tafuni et al., 2018) within DualSPHysics is also increasingly well tested for wave generation and absorption (Verbrugghe et al., 2019). Recently, a combination of open boundaries for wave generation and a damping zone for wave absorption has been demonstrated for current generation without a damping zone and wave–current generation and absorption with a modified damping zone acting on the vertical velocity component in Yang et al. (2023a). Taking advantage of open boundary conditions, the imposed physical quantities at the inlet can be from theoretical solutions, experiments and other numerical tools to replicate various complex flow conditions. This combination is further used for the investigation of numerical modelling of waves and sheared currents with a vertical cylinder in Yang et al. (2023b). A similar combined use of inlet-outlet boundary conditions and a damping zone for modelling a moored wave buoy in waves and currents in DualSPHysics using a third-order higher approximation was presented in Capasso et al. (2023). Offshore floating structures with a mooring system in waves were investigated in DualSPHysics considering a wave energy converter in Tagliafierro et al. (2022) and a floating offshore wind turbine with a focus on hydrodynamic motions in Tan et al. (2023) and hydrodynamic loads in Tagliafierro et al. (2023).

Fluid–structure interactions considering elastic structures can also be investigated based on the SPH method including the WCSPH-based DualSPHysics. Several test cases including violent free-surface flows interacting with elastic structures were validated in Khayyer et al. (2018) using an enhanced ISPH method and in Khayyer et al. (2021) using an enhanced multi-resolution ISPH solver. Test cases for elastic structures were also validated in Sun et al. (2019) and Sun et al. (2021) using an FSI-SPH model based on WCSPH, and in O'Connor and Rogers (2021) by manipulation of the existing boundary condition within DualSPHysics. Using a coupling between DualSPHysics and Project Chrono (Tasora et al., 2016), an elastic structure impacted by the dam break flow was validated in Capasso et al. (2022) and an elastic blade under the action of an oscillatory flow was validated in El Rahi et al. (2023).

In this paper, to generate the extreme wave conditions in the SPH numerical model to replicate the experimental investigation

(Esandi et al., 2020) in the physical flume, the combination of open boundaries and a damping zone is implemented for wave generation and absorption. The time histories of the surface elevation and flow kinematics used as boundary conditions at the inlet of the SPH numerical model are pre-computed using another Lagrangian numerical model (Buldakov et al., 2006, 2015) to replicate the experiments, hereby referred to as the Buldakov et al. model. The model simulates 2-D inviscid free-surface flows in Lagrangian coordinates. The formulation includes the Lagrangian continuity equation, the Lagrangian form of vorticity conservation and the dynamic free-surface condition and is solved using a finite difference approximation. For the controlled generation of near-breaking waves and spilling breaking waves, an iterative wave focusing methodology (Buldakov et al., 2017) was used within the Buldakov et al. model and the experiments. Validating the numerical model's ability at capturing the secondary load cycle and obtaining the higher-mode vibrations in a cylinder being impacted by waves are the two important scopes in the present study and have received no attention to date using the SPH method. The numerical results from the SPH model generated in empty flume are compared with the Buldakov et al. model for surface elevations and velocity profile and compared with experimental measurements with a cylinder in place (wave probes are installed 40 cm from the flume sidewall, away from the cylinder with just a slightly disturbed incoming wave) for surface elevations to validate the accuracy of the generated extreme wave conditions. Then, the numerical results from the SPH model are validated with experimental measurements of horizontal forces on the vertical cylinder. Finally, a dynamic model for the cylinder is used to study the response to extreme wave events.

This paper is organised as follows: in Section 2, the SPH model is outlined. In Section 3, the experimental setup and the numerical setup are given. In Section 4, the numerical results are compared with the experimental measurements including surface elevation and cylinder loading for model validation. In Section 5, the dynamic response of the cylinder to near-breaking and spilling breaking waves is studied. In Section 6, the conclusions and future work are provided.

2. Smoothed particle hydrodynamics model

SPH is a Lagrangian and meshless method which is increasingly used for fluid flows. The basic idea of the SPH method is that the fluid domain is discretised into a set of particles, each of which carries its own physical properties (e.g., density, velocity, pressure, acceleration). Physical quantities of each particle are computed as the interpolation of the values of the neighbouring particles. These particles are moved according to the combined action of internal forces (pressure gradient, viscous forces, etc.) and external forces (gravity force, etc.). The developments and advances of SPH will not be given in detail here, and they can be found in review articles (e.g., Violeau and Rogers, 2016; Gotoh and Khayyer, 2016; Wang et al., 2016; Shadloo et al., 2016; Ye et al., 2019; Luo et al., 2021).

The solver used for modelling a vertical cylinder exposed to near-breaking and spilling breaking waves is the SPH-based DualSPHysics code (Domínguez et al., 2022). In SPH, a function f at position $\mathbf{r}$ can be estimated by the integral approximation as:

$$\langle f(\mathbf{r})\rangle = \int_{\Omega} f(\mathbf{r}')W(\mathbf{r}-\mathbf{r}',h)\mathrm{d}\mathbf{r}' \tag{1}$$

where the integral is over the domain Ω, $W(\mathbf{r}-\mathbf{r}',h)$ is the kernel function and h is the smoothing length. In the discrete form, the integral approximation can be transformed approximately as:

$$f(\mathbf{r}_a) \approx \sum_b f(\mathbf{r}_b)\frac{m_b}{\rho_b}W(\mathbf{r}_a-\mathbf{r}_b,h) \tag{2}$$

where m_b/ρ_b is the volume of particle b with m_b and ρ_b being the particle mass and particle density respectively, and $W(\mathbf{r}_a-\mathbf{r}_b,h)$ is the kernel function between particle a and particle b. Note, for simplicity below a function $f(\mathbf{r}_b)$ is written as f_b.

2.1. SPH governing equations

The continuity equation and momentum equation in Lagrangian form can be written as:

$$\frac{\mathrm{d}\rho}{\mathrm{d}t} = -\rho\nabla\cdot\mathbf{v} \tag{3}$$

$$\frac{\mathrm{d}\mathbf{v}}{\mathrm{d}t} = -\frac{1}{\rho}\nabla P + \mathbf{g} + \mathbf{\Gamma} \tag{4}$$

where t is time, ρ is density, $\mathbf{v}$ is velocity, P is pressure, $\mathbf{g}$ is gravitational acceleration and $\mathbf{\Gamma}$ refers to dissipative terms. In SPH form, Eq. (3) including the density diffusion term and Eq. (4) can be written as:

$$\frac{\mathrm{d}\rho_a}{\mathrm{d}t} = \rho_a\sum_b\frac{m_b}{\rho_b}\mathbf{v}_{ab}\cdot\nabla_a W_{ab} + \delta h c_a\sum_b\frac{m_b}{\rho_b}\mathbf{\Psi}_{ab}\cdot\nabla_a W_{ab} \tag{5}$$

$$\frac{\mathrm{d}\mathbf{v}_a}{\mathrm{d}t} = -\sum_b m_b\left(\frac{P_b+P_a}{\rho_b\rho_a}+\Pi_{ab}\right)\nabla_a W_{ab} + \mathbf{g} \tag{6}$$

where m is mass, W is the kernel function, h is the smoothing length, c is the speed of sound, and δ is the free parameter which needs to

be selected and the value 0.1 as recommended in Antuono et al. (2010) is used in the present study. To avoid unphysical fluctuations in the pressure field, the density diffusion term $\mathbf{\Psi}_{ab}$ applied in Eq. (5) is that of Fourtakas et al. (2019) and is given by:

$$\mathbf{\Psi}_{ab} = 2\left(\rho_{ba}^{T} - \rho_{ab}^{H}\right)\frac{\mathbf{r}_{ab}}{|\mathbf{r}_{ab}|^2} \tag{7}$$

where superscript T and H denote the total and hydrostatic component respectively. The use of artificial viscosity (Monaghan, 1992) in Eq. (6) is a common stabilizing method in SPH and the viscosity term Π_{ab} is given by:

$$\Pi_{ab} = \begin{cases} \dfrac{-\alpha\overline{c_{ab}}\mu_{ab}}{\overline{\rho_{ab}}} & \mathbf{v}_{ab}\cdot\mathbf{r}_{ab} < 0 \\ 0 & \mathbf{v}_{ab}\cdot\mathbf{r}_{ab} \geq 0 \end{cases} \tag{8}$$

where $\overline{c_{ab}} = (c_a + c_b)/2$ is the mean speed of sound, $\overline{\rho_{ab}} = (\rho_a + \rho_b)/2$, $\mu_{ab} = h\mathbf{v}_{ab}\cdot\mathbf{r}_{ab}/(r_{ab}^2 + 0.01h^2)$, and α is the coefficient to provide stabilizing dissipation and the value 0.001 is selected to provide a slight dissipation in the present study. The kernel function W used is the quintic Wendland kernel (Wendland, 1995) given by:

$$W(r,h) = \alpha_D\left(1 - \frac{q}{2}\right)^4(2q+1)\ 0 \leq q \leq 2 \tag{9}$$

where α_D is $7/(4\pi h^2)$ in 2-D and $21/(16\pi h^3)$ in 3-D, $q = r/h$ is the non-dimensional distance between particles with r is the distance between two particles a and b. The smoothing length is set equal to $h = 1.5 \times \sqrt{3} \times d_p$ with d_p the initial interparticle distance. In WCSPH, an equation of state is used to determine the fluid pressure based on the particle density. In the present study, the relationship between pressure and density is given by Morris' equation of state:

$$P = c_0^2(\rho - \rho_0) \tag{10}$$

where ρ_0 is the reference density which equals to 1000 kg/m^3 and c_0 is the speed of sound at the reference density. The speed of sound 76 m/s is used in the present study to ensure the weakly compressible fluid and also a reasonable time step. Eq. (10) is used in several studies (Antuono et al., 2012; Sun et al., 2015) to reduce noise in the pressure field. Eqs. (5) and (6) and the particle position are updated using the symplectic time-stepping method with time step criterion given a CFL value of 0.5 in the present study (Leimkuhler and Matthews, 2015).

2.2. Boundary conditions

Open boundary conditions introduced in Tafuni et al. (2018) are applied in the present study for the generation of near-breaking and spilling breaking waves. The use of open boundary conditions is described in more detail in Section 3.2. Modified dynamic boundary conditions (mDBC) introduced in English et al. (2022) are applied in the present study to avoid the unphysical gap between fluid and boundary. Periodic boundary conditions (PBC) with a detailed description in Domínguez et al. (2022) are applied in the present study instead of solid side walls to avoid a large width of the physical flume. The general sketch of boundary conditions for modelling a vertical cylinder in extreme wave conditions is shown in Fig. 1.

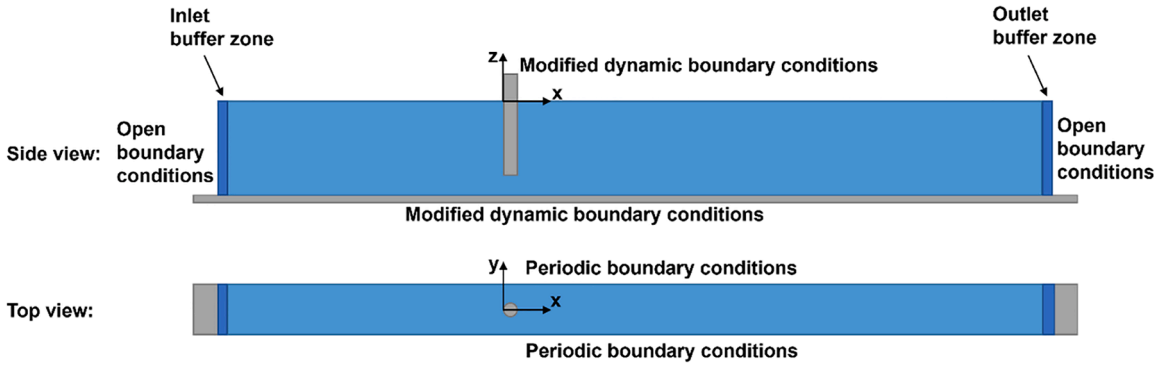

Fig. 1. General sketch of boundary conditions used in the numerical modelling. From top to bottom: side view and top view.

3. Experimental setup and numerical setup

Experimental investigations of the interaction of near-breaking and spilling breaking waves with a vertical cylinder were carried out in the physical flume at University College London (UCL). The experimental and numerical setup are presented in this section. The experimental measurements are used to validate the results of the SPH-based numerical model.

3.1. Experimental setup

The physical flume at UCL is 17 m long, 2.5 m wide, and 1.3 m deep with all experiments conducted in a water depth of 1 m. An array of seven flap wavemakers is arranged at one end of the flume and a full width parabolic beach is arranged at the other end. An iterative wave focusing methodology (Buldakov et al., 2017) was used in the experiments for the controlled generation of near-breaking and spilling breaking waves. One key feature of this methodology is using a linearised spectrum instead of a full spectrum as an output of the iterative focusing process. The second key feature is that wave records at different positions are used for amplitude and phase iterations, the former is referred to as the amplitude matching point (AMP) and the latter is referred to as the focal point (FP). For the detailed descriptions of the iterative wave focusing methodology the reader can refer to Buldakov et al. (2017). In the experiment, the AMP is 3 m from the wave generator and the FP is 11 m from the wave generator. In the present study, the FP is defined at $x = 0$ m and the time of linear focus is defined as $t = 0$ s.

Focused waves were generated using a Gaussian target spectrum with peak periods of 1.2 s and 1.4 s. For each wave period, the iterative procedure was applied to create a series of waves with different linear focused amplitudes. Surface elevation of a target wave group at $x = 0$ m is defined as:

$$\eta(t) = A\int_0^\infty S(\omega)\cos(\omega t + \Phi(\omega))\mathrm{d}\omega \tag{11}$$

where A is a linear focused amplitude and $\Phi(\omega) = 0$ is set for a crest focused wave. A normalised Gaussian amplitude spectrum is:

$$S(\omega) = \frac{1}{\omega_p\sigma\sqrt{2\pi}}\exp\left(-\frac{1}{2\sigma^2}\left(\frac{\omega}{\omega_p}-1\right)^2\right) \tag{12}$$

where ω_p is a peak angular frequency. A parameter σ is used to control the bandwidth of the spectrum and $\sigma = 0.2898$ is used. This provides a spectrum that occupies a range of frequencies from $\omega = 0$ to $\omega = 2\omega_p$ ($\omega_p = 5.236$ rad/s for $T_p = 1.2$ s and $\omega_p = 4.488$ rad/s for $T_p = 1.4$ s) and parts of the spectrum beyond this range are neglected. Five wave groups for each period including steep non-breaking waves and breaking waves are selected for tests with the cylinder in the experiments. Among them, there are three non-breaking cases and two breaking cases. A cylinder with a diameter of 0.165 m was installed as the test model. The front line of the cylinder was located at the FP at the centre line of the flume. A general sketch of the physical flume is adapted from Esandi et al. (2020) and shown in Fig. 2. In the present study, the largest non-breaking case and two spilling breaking cases for each period are selected for the numerical model validation. The parameters of the selected waves are shown in Table 1. For the detailed descriptions of the

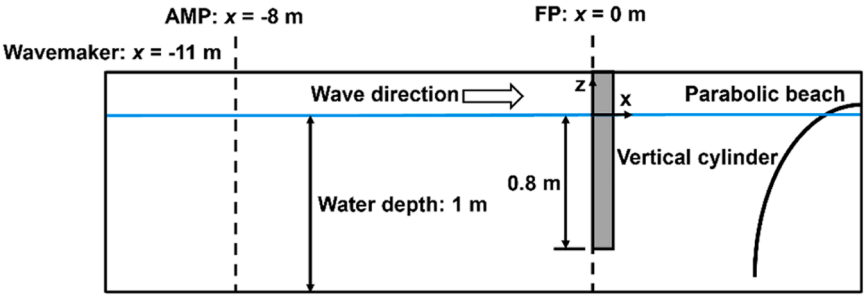

Fig. 2. General sketch of the physical flume at UCL, modified from Esandi et al. (2020).

Table 1
Test cases.

Test number	Linear target focused amplitude A_f [m]	Peak period T_p [s]	Peak wavelength L_p [m]	k_pA_f	Wave behaviour
1. T12NB3	0.098	1.2	2.23	0.275	Non-breaking
2. T12BR1	0.1015	1.2	2.23	0.285	Breaking
3. T12BR2	0.105	1.2	2.23	0.295	Breaking
4. T14NB3	0.135	1.4	2.97	0.285	Non-breaking
5. T14BR1	0.1395	1.4	2.97	0.294	Breaking
6. T14BR2	0.144	1.4	2.97	0.304	Breaking

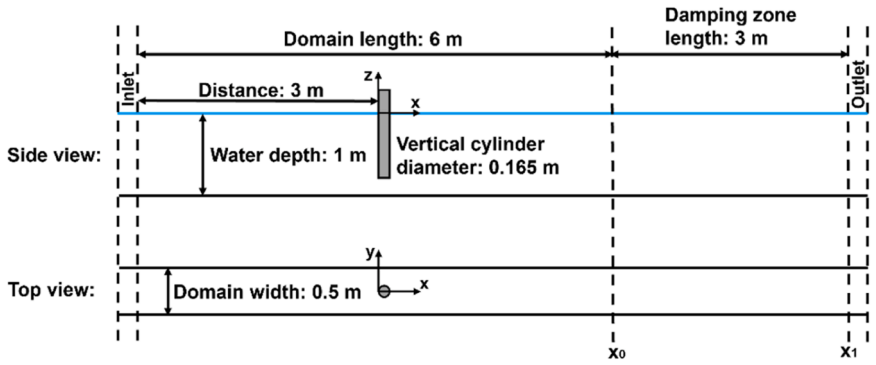

Fig. 3. General sketch of the SPH numerical model. The origin is located at the front line of the cylinder, the centre line of the flume and the undisturbed free surface. From top to bottom: side view and top view.

experimental setup the reader can refer to Esandi et al. (2020).

The surface elevation was measured by 2 wave probes installed at the AMP and FP and 40 cm from the flume sidewall. The iterative wave focusing methodology was applied within the Buldakov et al. model and outputs from this model are used as boundary conditions at the inlet of the SPH numerical model to replicate the experiments. This combined model approach with fully nonlinear kinematics enables a truncated numerical wave flume compared with the physical flume owing to a full development of the wave conditions within this distance before interacting with the cylinder. Thus, only the surface elevation measured at the FP in the experiments is used for the numerical model validation since the inlet of the numerical wave flume to the cylinder is at $x = -3$ m (the AMP is defined at $x = -8$ m).

3.2. Numerical setup

For the numerical model, the domain length is 6 m ($L_{domain}/L_p \approx 2.7$ for $T_p = 1.2$ s, $L_{domain}/L_p \approx 2.0$ for $T_p = 1.4$ s), the damping zone length is 3 m as it is recommended to use one wavelength (peak wavelengths are 2.97 m and 2.23 m corresponding to the two different peak periods) as the length of the damping zone (Altomare et al., 2017), the water depth is 1 m, and the domain width is 0.5 m instead of 2.5 m in the physical flume by taking advantage of PBC as reflection from the solid side wall will affect the results. For wave–structure interaction tests, the front line of the vertical cylinder (diameter $D = 0.165$ m) is located at the FP ($x = 0$ m) which is 11 m from the wavemaker in the physical flume and is 3 m from the inlet in the SPH numerical flume. A general sketch of the SPH numerical model is shown in Fig. 3.

Open boundaries are applied for the generation of extreme wave conditions. At both the inlet and the outlet, horizontal velocities and surface elevation are imposed and density is extrapolated from the fluid domain. At the inlet, no accuracy improvement can be obtained by imposing vertical velocities, but a negative influence on the particle spacing can occur (Ni et al., 2018; Verbrugghe et al., 2019). Using at least 8 layers of buffer particles arranged in buffer zones is suggested in Verbrugghe et al. (2019) to give accurate wave propagation simulations and this value is used in the present study. Following the methodology presented in Yang et al. (2023a) and Yang et al. (2023b), the buffer zone at the inlet is divided into 8 vertical sections in the present study. In each vertical section, the horizontal velocities (time series) are imposed at 3 different heights. At each instant, the horizontal velocities at other heights for this section are obtained according to a parabolic fit function of DualSPHysics. For the detailed description of the buffer zone at the inlet the reader can refer to Yang et al. (2023a) and Yang et al. (2023b).

A damping zone is arranged before the outlet in the numerical model. In DualSPHysics, the velocity is reduced in the damping zone according to:

$$\mathbf{v} = \mathbf{v}_0 \cdot f(x, \Delta t) \tag{13}$$

$$f(x, \Delta t) = 1 - \Delta t \cdot \beta \cdot \left(\frac{x - x_0}{x_1 - x_0}\right)^2 \tag{14}$$

where $\mathbf{v}_0$ is the initial velocity of the particle, $\mathbf{v}$ is the final velocity of the particle, $f(x, \Delta t)$ is the reduction function, x is the position of particles, Δt is the duration of the last time step, x_0 and x_1 are the initial and the final position of the damping zone respectively as shown in Fig. 3, β is the coefficient to modify the reduction function and the value is set equal to 10 in the present study.

4. Model validation

The implementation of the SPH-based numerical model for prediction of wave forces on the vertical cylinder due to near-breaking and spilling breaking waves is validated in this section. Firstly, the extreme wave conditions generated in an empty flume are validated with the Buldakov et al. model for surface elevation and velocity profile (it is an empty flume both in the SPH numerical model and the

Buldakov et al. model) and validated with the experiments with the cylinder in the physical flume for surface elevation (wave probes are installed 40 cm from the flume sidewall, away from the cylinder with just a slightly disturbed incoming wave) to demonstrate the accuracy of generation of extreme wave conditions. Then, the numerical modelling of interactions of extreme waves with the cylinder is validated with experiments for horizontal wave force on the cylinder to demonstrate the model's capability for modelling interactions of extreme waves with structures.

4.1. Wave conditions

The surface elevation is measured at the FP ($x = 0$ m). At the FP, the horizontal velocity profile is analysed at the time when surface elevation reaches the peak value in the numerical modelling. The numerical surface elevations are compared with the Buldakov et al. model (referred to as LaNM in the figure legends) and the experiments (referred to as EXP in the figure legends) in Fig. 4. At the FP, the numerical horizontal velocity profiles at the time of maximum elevation for each case according to SPH results are compared with the Buldakov et al. model in Fig. 5. To distinguish between the time-domain comparison and the spatial comparison, different line colours

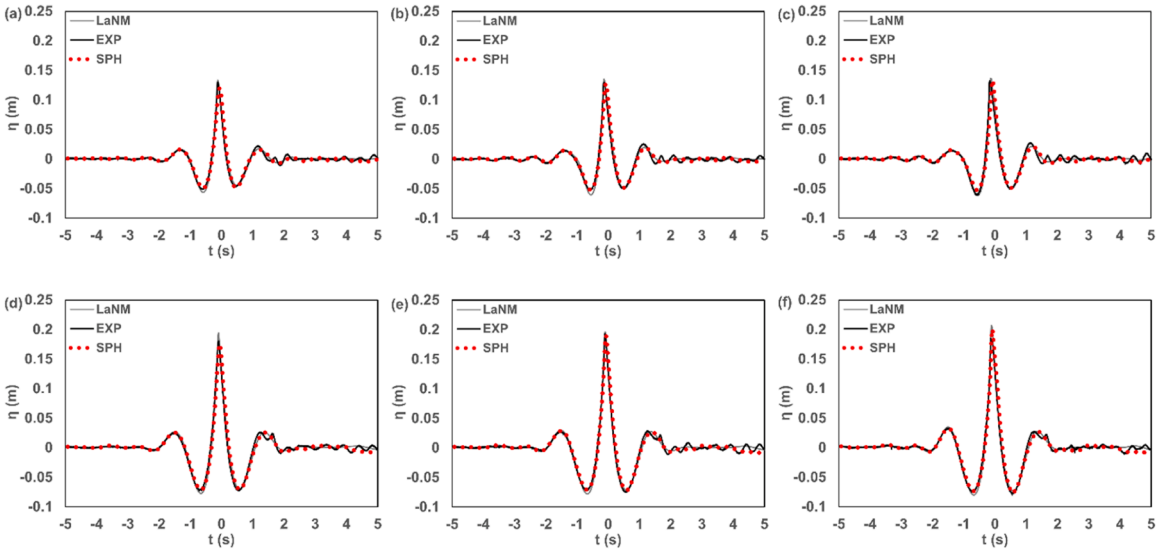

Fig. 4. Results of surface elevation in the SPH numerical model, in the Buldakov et al. model and in the experiments (a) case T12NB3, (b) case T12BR1, (c) case T12BR2, (d) case T14NB3, (e) case T14BR1, (f) case T14BR2.

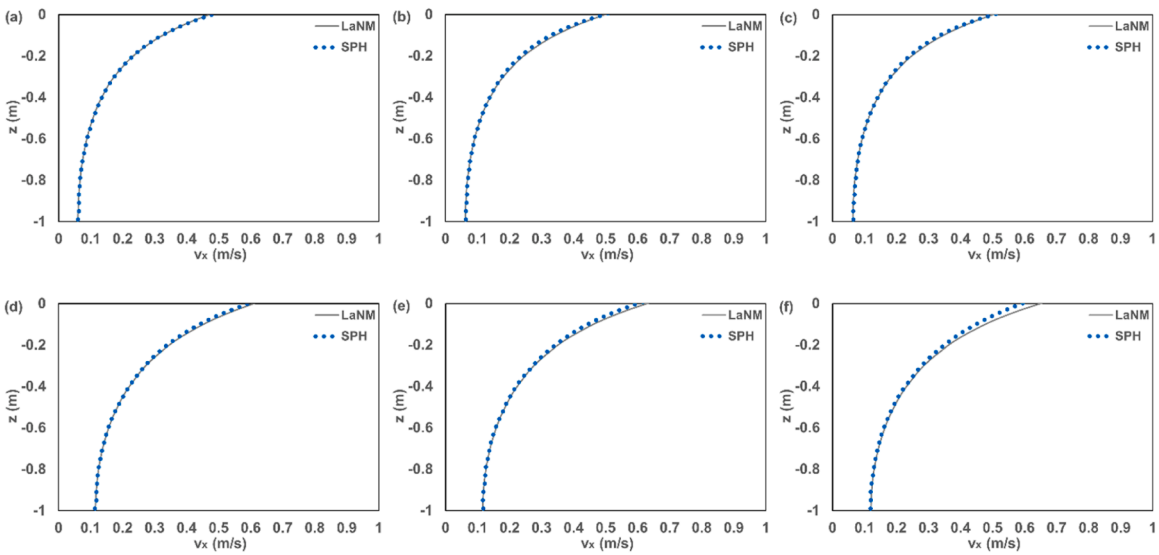

Fig. 5. Results of horizontal velocity profile in the SPH numerical model and in the Buldakov et al. model at the FP and the time of maximum elevation according to SPH results (a) case T12NB3, (b) case T12BR1, (c) case T12BR2, (d) case T14NB3, (e) case T14BR1, (f) case T14BR2.

for the SPH results are used in Figs. 4 and 5. Previous particle refinement studies showing convergence for focused waves can be found in Yang et al. (2023a) and showing convergence for wave forces acting on the cylinder can be found in Yang et al. (2023b). The initial interparticle distance d_p (= 0.0125 m) is used in the simulations presented in Section 4 which is also used in the model validation and provide accuracy in the particle refinement study in Yang et al. (2023b). According to Figs. 4 and 5, the extreme wave conditions generated in the physical flume are well replicated in the SPH-based numerical model using the outputs from the Buldakov et al. model. Some small fluctuations shown after the crest behind the main crest in the experiments indicate a slightly disturbed incoming wave after the main wave crest interacts with the cylinder. Thus, it is reasonable to include them in the comparison. For surface elevation in case T12NB3, the result indicated that the Buldakov et al. model gives a better agreement with the experiments although the difference between each model is small and within expected error bounds. An overall good agreement is achieved with some mismatch for velocity profile in case T14BR2 compared with the Buldakov et al. model.

4.2. Wave forces

The measured horizontal forces on the cylinder from the SPH numerical model are compared with those measured in the experiments in Fig. 6. The spikes in the experimental measurements are due to noise in the force measurements. The particles of the cylinder are arranged in terms of radial arrangement instead of Cartesian arrangement in the present study same as in Yang et al. (2023b) as suggested in Chow et al. (2019) for the simulation of interaction of focused waves interacting with a cylinder using ISPH. In addition to Fig. 6, the positive peak horizontal force at different focused amplitude (listed in Table 1) is given for all cases in Fig. 7. Compared with other cases, the SPH model overpredicts the positive peak horizontal force as also shown in Fig. 6 for case T14NB3. An overall good agreement is achieved between the numerical results and the experimental measurements. It can be seen that with the increase of the

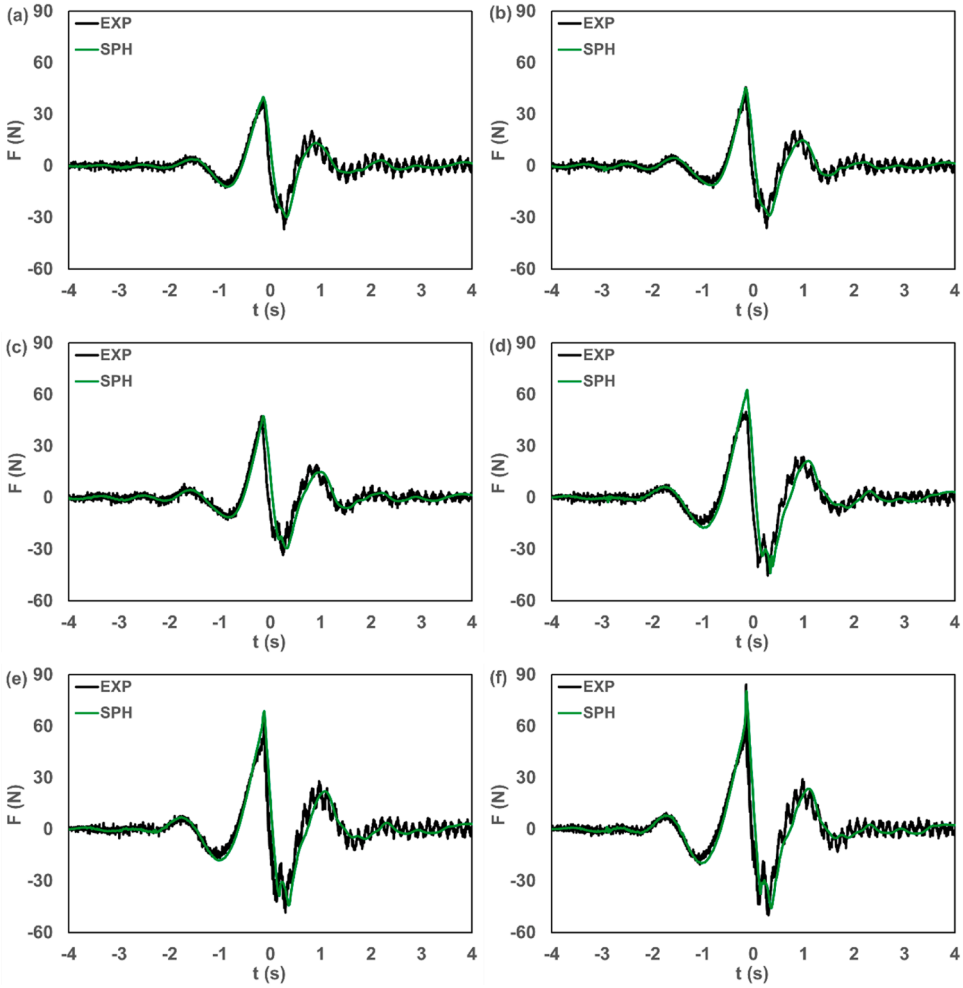

Fig. 6. Results of horizontal force in the SPH numerical model and in the experiments (a) case T12NB3, (b) case T12BR1, (c) case T12BR2, (d) case T14NB3, (e) case T14BR1, (f) case T14BR2.

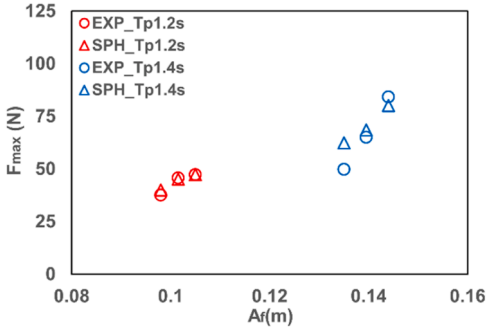

Fig. 7. Results of positive peak horizontal force at different focused amplitude in the SPH numerical model and in the experiments for cases T12NB3, T12BR1, T12BR2, T14NB3, T14BR1 and T14BR2.

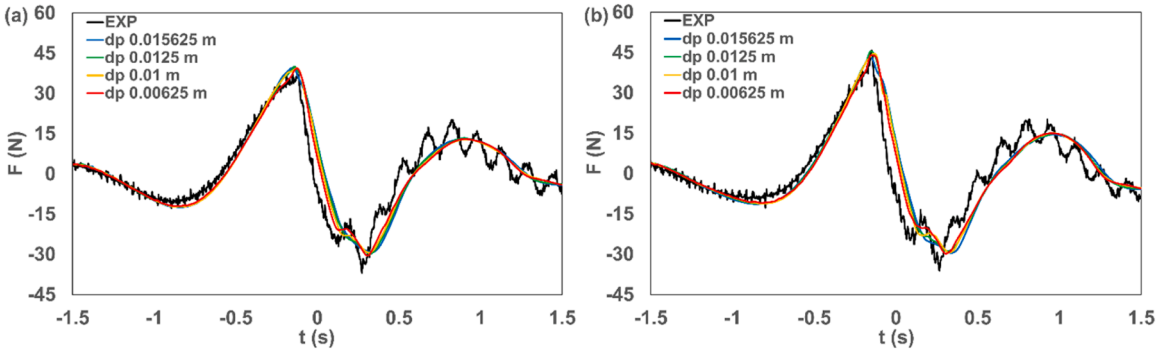

Fig. 8. Results of horizontal force using four different resolutions in the SPH numerical model (a) T12NB3, (b) T12BR1.

steepness, breaking wave forces are significantly larger compared with non-breaking wave forces for cases T14NB3, T14BR1 and T14BR2 (an increase is also observed for cases T12NB3, T12BR1 and T12BR2). The potential reason for a significantly larger increase of forces for the breaking cases for $T_p = 1.4$ s compared with the breaking cases for $T_p = 1.2$ s is due to different degrees of breaking affecting the impact force. However, it is consistent with other experimental investigations (e.g., Ji et al., 2015) that the wave force increases as the wave steepness increases.

The secondary load cycle formation shortly after the passage of the steep wave is well captured in SPH model for cases T12BR2, T14NB3, T14BR1 and T14BR2. It is consistent with the experimental findings in Li et al. (2022) that the secondary load cycle occurrence strongly depends on the wave steepness. For cases T12NB3 and T12BR1, there is no obvious secondary load cycle found in the SPH numerical results but shown in the experiments. To address this, a finer resolution d_p ($= 0.00625$ m), a moderately finer resolution d_p ($= 0.01$ m) and a coarser resolution d_p ($= 0.015625$ m) are used for cases T12NB3 and T12BR1. Values of d_p were selected so that the ratio d/d_p (d is the water depth) is an integer which is recommended in Altomare et al. (2017). The results shown in Fig. 8 highly indicated that the slight secondary load cycle could be detected using a finer resolution in the present SPH model. Therefore, the existence of the secondary load cycle is well predicted, but not the magnitude. However, the prediction of the magnitude of the secondary load cycle can be improved and is demonstrated later in Section 5. Though a truncated numerical model is used for the model validation compared with the physical flume, the particle number is 2.51×10^6 with runtime around 6 h (for 15 s of physical time) for $d_p = 0.0125$ m and is 4.82×10^6 with runtime more than 15 h for $d_p = 0.01$ m. For $d_p = 0.00625$ m, the particle number is 1.92×10^7 with runtime more than 22 h (computed on an Nvidia GeForce RTX 4090 GPU, all other simulations were computed on an Nvidia GeForce RTX 3080 Laptop GPU). Considering the agreement achieved between numerical results and the experimental measurements of the peak force, of most interest, using $d_p = 0.0125$ m presented in Section 4 and negligible difference using $d_p = 0.00625$ m and $d_p = 0.01$ m shown in Fig. 8, the initial interparticle distance d_p ($= 0.0125$ m) was still used in Section 5 computing on an Nvidia GeForce RTX 3080 Laptop GPU.

As found in Esandi et al. (2020) for cases T12BR2 and T12NB1 (not included in the present study with A_f equals to 8.4 cm), and T14BR2 and T14NB1 (not included in the present study with A_f equals to 11.7 cm), the maximum force in breaking waves is dominated by the wave crest impact in cases T12BR2 and T14BR2 whilst the time histories of force and surface elevation are out of phase for non-breaking waves in cases T12NB1 and T14NB1. It is also true in the present SPH model as shown in Fig. 9. The lag of peak values in time histories of surface elevation and force for highly nonlinear near-breaking waves and spilling breaking waves is almost disappeared. In Fig. 10, the simulation snapshots of the horizontal velocity field at the instant with the maximum force (the positive peak horizontal force) in the SPH model are shown demonstrating that for breaking cases the peak load occurs close to the time of wave crest impact.

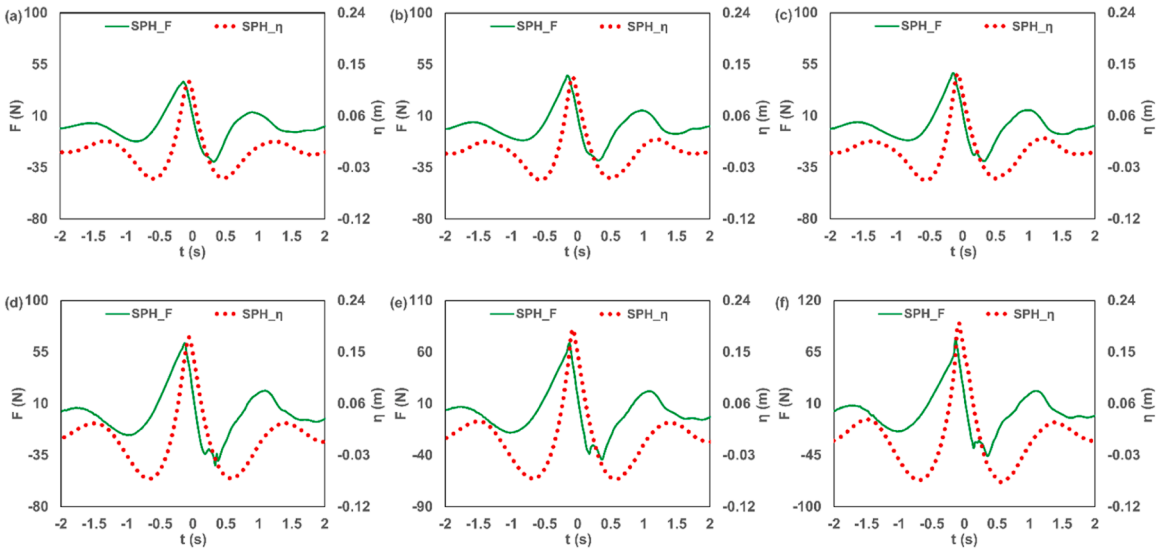

Fig. 9. Time histories of surface elevation and horizontal force (a) case T12NB3, (b) case T12BR1, (c) case T12BR2, (d) case T14NB3, (e) case T14BR1, (f) case T14BR2.

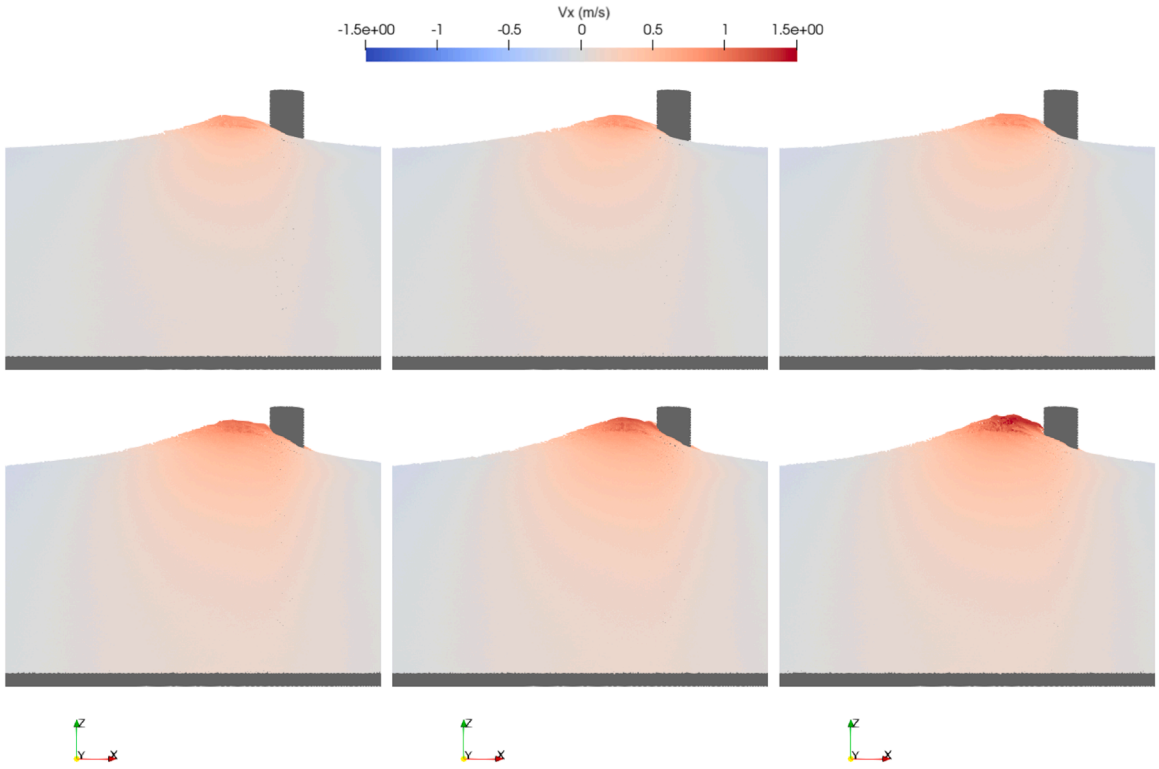

Fig. 10. Simulation snapshot of the horizontal velocity field at the instant when cylinder subject to positive peak horizontal force. From left to right in the top line: case T12NB3, case T12BR1 and case T12BR2. From left to right in the bottom line: case T14NB3, case T14BR1 and case T14BR2.

5. Dynamic response

The dynamic response of the cylinder to near-breaking and spilling breaking waves and its effect on the wave force is further investigated in this section. Firstly, the methodology for developing a dynamic cylinder model based on the present SPH numerical flume is given. Then, the interaction of extreme waves with the dynamic cylinder model is investigated to demonstrate the model's capability for considering the higher-mode vibrations in an object being impacted by waves using the SPH method.

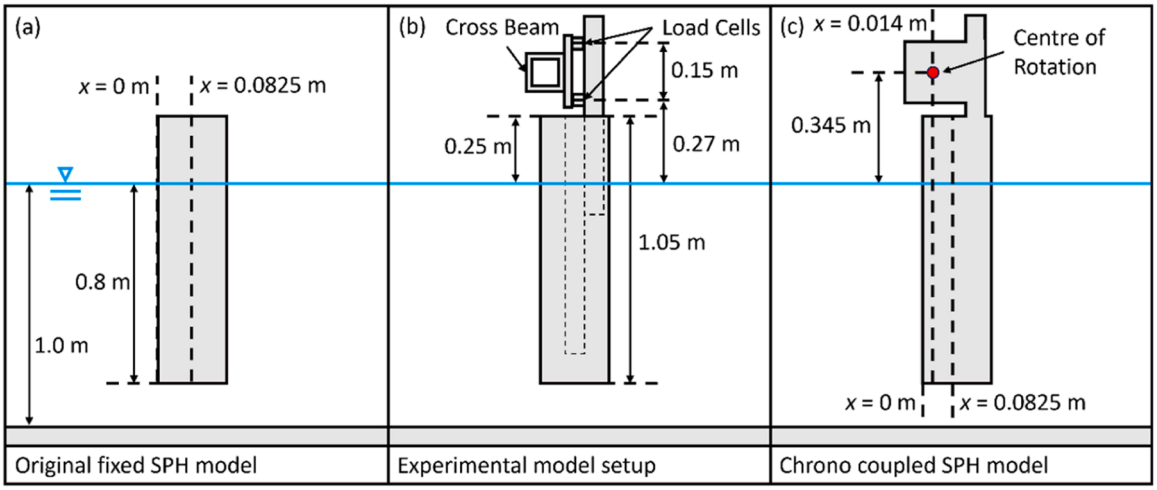

Fig. 11. Sketch of the two models and the experimental setup. (a) Original fixed SPH model set up consisting of cylinder fixed in place. (b) Sketch of experimental model setup showing location of cross beam and load cells. (c) Chrono coupled SPH model showing the location of the centre of rotation.

5.1. General development of a dynamic model

In the experiments of Esandi et al. (2020) it was noted that the cylinder being impacted by the waves was fixed in place by a steel beam across the channel, and that the first natural frequency of the structural system tested was around 6.5 Hz. Esandi et al. (2020) state that this dynamic response is the source of the higher order force oscillations seen in the experimental result after impact from the wave. This dynamic response, however, is not captured by the SPH model results shown in Section 4 as the cylinder is assumed to be fixed in place in the numerical model. Coupled to the DualSPHysics package, used for the SPH simulations in Section 5, is a powerful open-source multi-body solver called Project Chrono (Tasora et al., 2016), first incorporated into the solver by Canelas et al. (2018). Coupling between the latest version of DualSPHysics with Project Chrono to solve complex fluid–solid interaction problems is provided in Martínez-Estévez et al. (2023). Project Chrono works in DualSPHysics by allowing solid bodies to move, collide and rotate subject to constraints and restrictions such as joints, hinges and springs. A fast Fourier transform (FFT) analysis of the experimental results found a second peak in the frequency domain at a frequency of 6.466 Hz, in close agreement with the 6.5 Hz calculated by Esandi et al. (2020). Using this natural frequency and Project Chrono, the dynamic response of the cylinder due to the impact of the wave can be studied numerically based on the SPH method and validated against the experimental measurements for the first time.

In DualSPHysics the combination of the cylinder, the supporting cross beam and the load cells can be introduced as a single so-called Chrono object in a similar way as the original cylinder was in Section 4, a sketch of the two models along with the experimental model setup are shown in Fig. 11. The centre of rotation for the Chrono cylinder was chosen to be approximately in the centre of the support beam, assumed to be the centre of rotation of the dynamic response of the cylinder. The centre of mass of the cylinder was then placed directly under the centre of rotation and halfway along the length of the cylinder to ensure the cylinder would hang straight in the absence of any fluid. A uniform mass distribution is assumed across the length of this model. The Chrono cylinder was modelled with a damped torsional oscillator, defined as a hinge joint in the DualSPHysics code, located at the centre of rotation, with the torsional stiffness k and torsional damping c used. Using a hinge is a close approximation to the experimental setup and it is simple to characterise based on the experimental data provided.

The torsional stiffness k is calculated as:

$$k = (2\pi f_n)^2 I \tag{15}$$

where f_n is the natural frequency in water and I is the moment of inertia of the object. The moment of inertia I is calculated as:

$$I = M_{dry}\left(H_{dry}^2 + \frac{L_{dry}^2}{12}\right) + M_{added}\left(H_{added}^2 + \frac{L_{added}^2}{12}\right) \tag{16}$$

where $M_{dry} = 11.5$ kg is the dry mass, $L_{dry} = 1.3$ m is the total dry length, $H_{dry} = 0.495$ m is the distance between the centres of the dry mass and rotation, $M_{added} = 17.106$ kg is the added mass of the water displaced by the cylinder, $L_{added} = 0.8$ m is the submerged depth, and $H_{added} = 0.745$ m is the distance from the submerged centre of mass to the centre of rotation. Thus, the moment of inertia $I = 14.844$ kg m^2, using a natural frequency $f_n = 6.466$ Hz, the torsional stiffness $k = 24{,}501$ N m/rad. There is no torsional damping used in the simulations, as there is inherent damping due to numerical viscosity in the simulations.

5.2. Wave forces with dynamic response

The measured horizontal forces on the cylinder from the SPH numerical model considering a dynamic cylinder model with the response are compared with those measured in the experiments in Fig. 12. In Fig. 13 the simulation snapshot of the pressure field at the instant with the maximum force (the positive peak horizontal force) in the SPH model with dynamic response for case T14BR2 is given. An FFT is applied to the time history of the horizontal force to obtain the amplitude spectra for both the fixed model and the dynamic model. They are compared with those from experimental measurements in Fig. 14. An overall good agreement is still achieved between the numerical results and the experimental measurements. Compared with using a fixed cylinder model as shown in Fig. 6, it can be seen that the secondary load cycle becomes obvious and larger for a dynamic cylinder model with the response due to the impact of the wave which gives a better agreement with the experimental measurements. It is indicated that there is a relationship between the magnitude of the secondary load cycle and the dynamic response. A peak value is also shown in the amplitude spectra for the dynamic model around the natural frequency in the experiments.

For a closer comparison, the measured horizontal forces on the cylinder (from −3 s to 3 s) from the SPH numerical model including both the fixed model and the dynamic model are compared with those measured in the experiments in Fig. 15. It is demonstrated that the high-frequency fluctuations in the time histories of the horizontal force which are directly linked to the higher-mode vibrations of the cylinder generated by the wave impact in the experiments are also captured in the SPH numerical model.

According to Fig. 15, the dynamic response of the cylinder has negligible effect on the phase of the peak force. In addition to Fig. 15, the positive peak horizontal force for both the fixed model and the dynamic model at different focused amplitude is given in Fig. 16. It is demonstrated that the dynamic response of the cylinder has a limited effect on the peak force in the present study since the natural frequency of the structural system (6.466 Hz) is far away from the peak wave frequency (0.833 Hz and 0.714 Hz) and the dynamic response only causes the higher order force oscillations in force measurements after impact from the wave. However, the SPH model with dynamic response provides a closer agreement with the experiments for the positive peak horizontal force for case T14BR1.

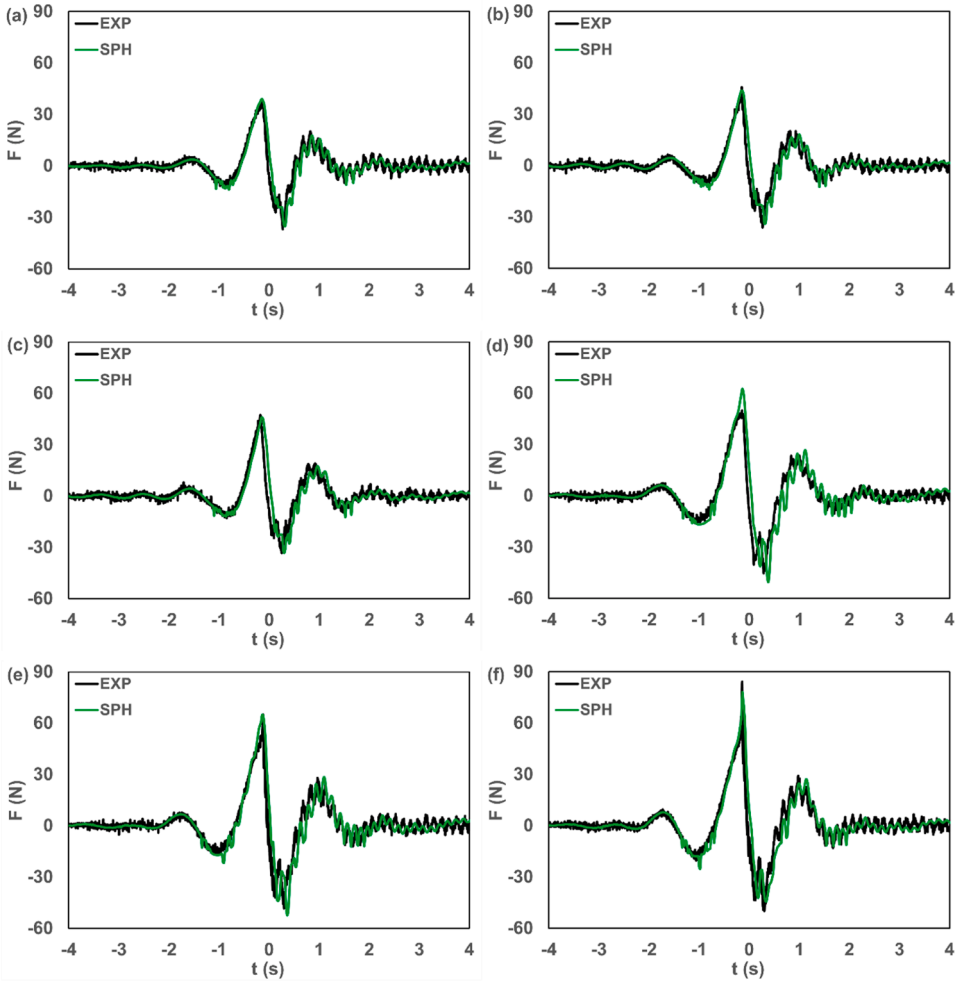

Fig. 12. Results of horizontal force in the SPH numerical model with dynamic response and in the experiments (a) case T12NB3, (b) case T12BR1, (c) case T12BR2, (d) case T14NB3, (e) case T14BR1, (f) case T14BR2.

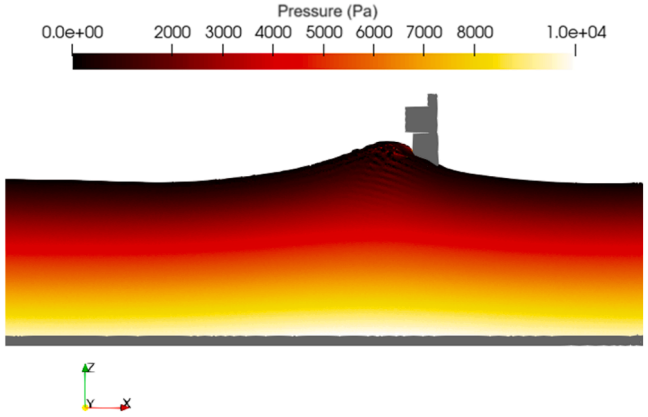

Fig. 13. Simulation snapshot of the pressure field at the instant when cylinder subject to positive peak horizontal force in the SPH numerical model with dynamic response for case T14BR2.

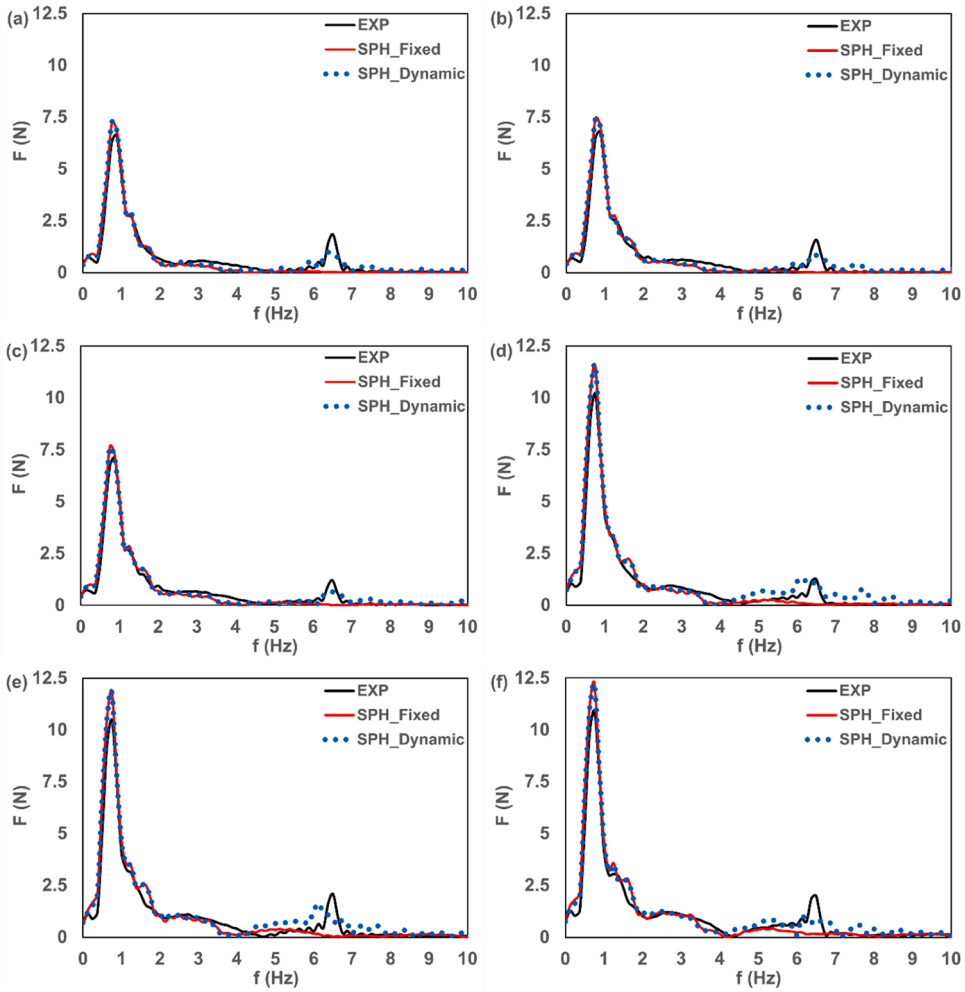

Fig. 14. Results of amplitude spectra of the horizontal force in the two SPH numerical models and in the experiments (a) case T12NB3, (b) case T12BR1, (c) case T12BR2, (d) case T14NB3, (e) case T14BR1, (f) case T14BR2.

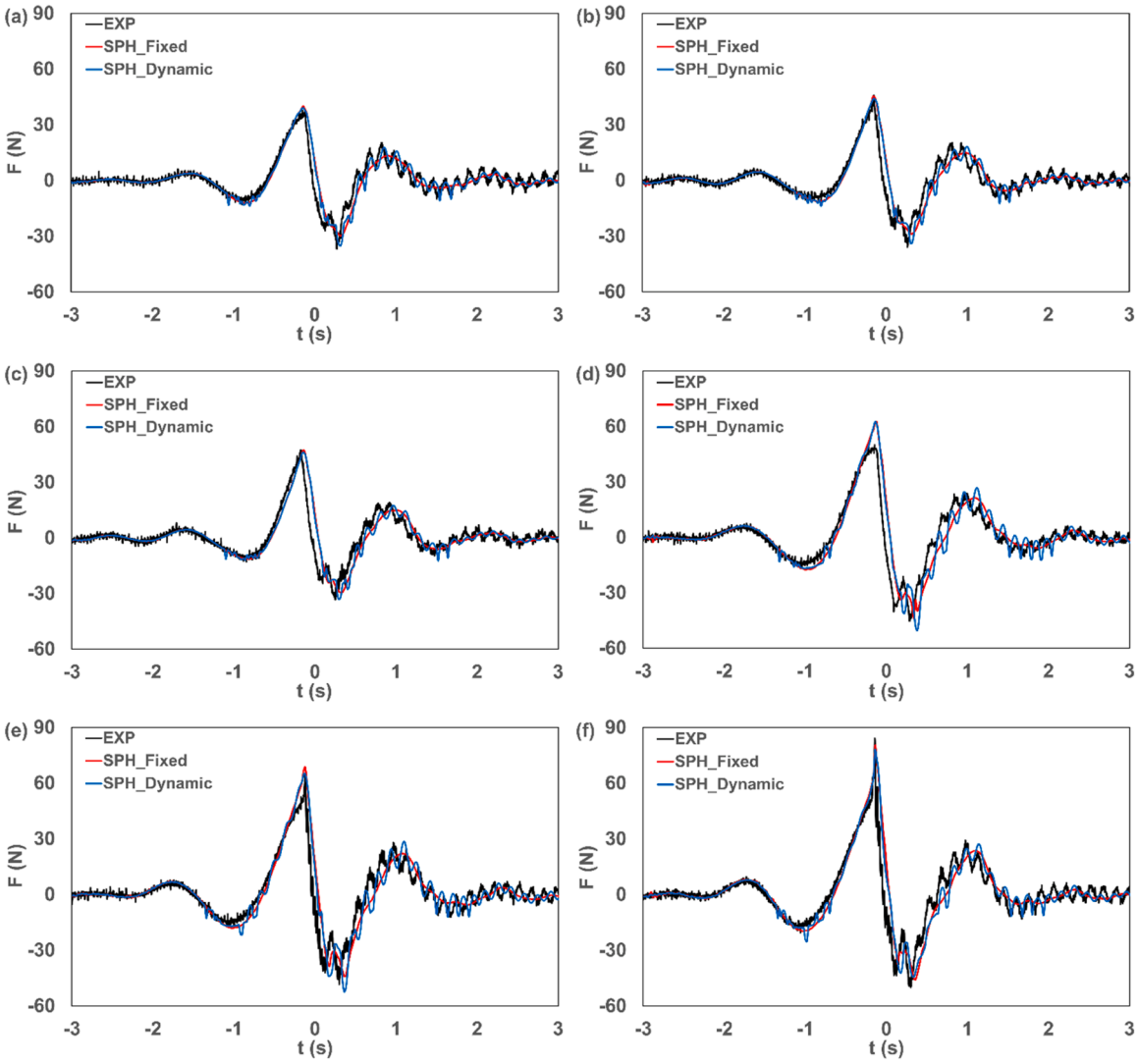

Fig. 15. Results of horizontal force in the two SPH numerical models and in the experiments (a) case T12NB3, (b) case T12BR1, (c) case T12BR2, (d) case T14NB3, (e) case T14BR1, (f) case T14BR2.

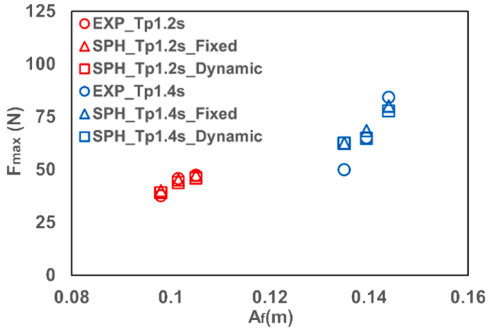

Fig. 16. Results of positive peak horizontal force at different focused amplitude in the two SPH numerical model and in the experiments for cases T12NB3, T12BR1, T12BR2, T14NB3, T14BR1 and T14BR2.

6. Discussion and conclusions

Prediction of loading on offshore and ocean structures is of great significance for engineering design and wave loading due to non-breaking waves has been extensively studied. However, no significant studies address on the effects of spilling breaking waves (Esandi et al., 2020). To develop a numerical model with the ability to address this problem, numerical modelling of a vertical cylinder exposed to near-breaking waves and spilling breaking waves using SPH-based DualSPHysics code has been presented in this paper. The advances of the SPH method for free-surface flows make it ideal for the present study. To generate the conditions in the SPH numerical model, a combination of open boundaries and a damping zone is implemented as in Yang et al. (2023a) and Yang et al. (2023b). Outputs from the Buldakov et al. model are used as the inputs of the SPH numerical model to replicate the extreme wave conditions generated in a physical flume in Esandi et al. (2020). This combined model approach allows a truncated numerical wave flume compared with the physical flume due to the use of fully nonlinear kinematics.

The extreme wave conditions generated in empty flume are validated with the Buldakov et al. model for surface elevation and velocity profile and the experiments with cylinder in the physical flume for surface elevation, demonstrating the accuracy of the method used for generation of extreme wave conditions. An overall good agreement is achieved for the horizontal wave forces on the cylinder between the numerical results from the SPH model and experimental measurements, demonstrating the model's capability in the present study for prediction of wave forces due to near-breaking waves and spilling breaking waves with a satisfactory computational performance by only using a laptop GPU. The larger breaking wave forces compared with highly nonlinear non-breaking wave forces and the secondary load cycle occurrence in highly nonlinear fluid–structure interaction which are found in many experimental investigations are well captured in the present SPH numerical model. The high nonlinearity involved in the slamming process shown in many experiments was also found in a former investigation (Yang et al., 2023b) of the present study. Therefore, a reliable numerical model as an effective tool for modelling complex and extreme fluid–structure interaction is achieved.

With the coupled use of a powerful open-source multi-body solver called Project Chrono, the vibration of the cylinder due to wave impact which occurred in the experiments is simulated using the SPH method and validated against the experimental measurements for the first time. The horizontal force time histories acting on the cylinder with the effect of the higher-mode vibrations of the cylinder due to the impact of the wave and the experimental measurements show an overall good agreement. It is noted that the secondary load cycle becomes larger with the correct dynamic response of the cylinder model compared with a fixed cylinder model. It is also shown that the forces due to near-breaking and spilling breaking waves have a significant effect on the design of offshore and ocean structures since they lead to high frequency vibrations of the structure. By considering a dynamic cylinder model with the response, the SPH-based model in the present study gives a powerful numerical approach to assess the loading and dynamic response of offshore and ocean structures in complex and extreme wave conditions including breaking waves.

CRediT authorship contribution statement

Yong Yang: Conceptualization, Formal analysis, Investigation, Methodology, Software, Validation, Writing – original draft, Writing – review & editing. **Aaron English:** Methodology, Software, Writing – review & editing. **Benedict D. Rogers:** Conceptualization, Methodology, Resources, Software, Supervision, Writing – review & editing. **Peter K. Stansby:** Conceptualization, Methodology, Resources, Software, Supervision, Writing – review & editing. **Dimitris Stagonas:** Conceptualization, Methodology, Resources, Writing – review & editing. **Eugeny Buldakov:** Conceptualization, Methodology, Resources, Writing – review & editing. **Samuel Draycott:** Conceptualization, Funding acquisition, Methodology, Resources, Supervision, Writing – review & editing.

Declaration of competing interest

The authors declare that they have no known competing financial interests or personal relationships that could have appeared to influence the work reported in this paper.

Data availability

Data will be made available on request.

Acknowledgments

The authors would like to acknowledge funding for this project from the School of Engineering at The University of Manchester. S. Draycott acknowledges a Dame Kathleen Ollerenshaw Fellowship.

References

Altomare, C., Crespo, A.J.C., Domínguez, J.M., Gómez-Gesteira, M., Suzuki, T., Verwaest, T., 2015. Applicability of Smoothed Particle Hydrodynamics for estimation of sea wave impact on coastal structures. Coast. Eng. 96, 1–12.

Altomare, C., Domínguez, J.M., Crespo, A.J.C., González-Cao, J., Suzuki, T., Gómez-Gesteira, M., Troch, P., 2017. Long-crested wave generation and absorption for SPH-based DualSPHysics model. Coast. Eng. 127, 37–54.

Antuono, M., Colagrossi, A., Marrone, S., 2012. Numerical diffusive terms in weakly-compressible SPH schemes. Comput. Phys. Commun. 183, 2570–2580.

Antuono, M., Colagrossi, A., Marrone, S., Molteni, D., 2010. Free-surface flows solved by means of SPH schemes with numerical diffusive terms. Comput. Phys. Commun. 181, 532–549.
Buldakov, E., Stagonas, D., Simons, R., 2015. Lagrangian numerical wave–current flume. In: Proceedings of the 30th International Workshop on Water Waves and Floating Bodies, 12th - 15th April, Bristol.
Buldakov, E., Stagonas, D., Simons, R., 2017. Extreme wave groups in a wave flume: controlled generation and breaking onset. Coast. Eng. 128, 75–83.
Buldakov, E.V., Taylor, P.H., Eatock Taylor, R., 2006. New asymptotic description of nonlinear water waves in Lagrangian coordinates. J. Fluid Mech. 562, 431–444.
Canelas, R.B., Brito, M., Feal, O.G., Domínguez, J.M., Crespo, A.J.C., 2018. Extending DualSPHysics with a Differential Variational Inequality: modeling fluid-mechanism interaction. Appl. Ocean Res. 76, 88–97.
Capasso, S., Tagliafierro, B., Martínez-Estévez, I., Domínguez, J.M., Crespo, A.J.C., Viccione, G., 2022. A DEM approach for simulating flexible beam elements with the Project Chrono core module in DualSPHysics. Comput. Part. Mech. 9, 969–985.
Capasso, S., Tagliafierro, B., González-Avalos, R., Martínez-Estévez, I., Domínguez, J.M., Altomare, C., Crespo, A.J.C., Viccione, G., 2023. Numerical simulation of a moored wave-buoy in waves and current by smoothed particle hydrodynamics. In: Proceedings of the ASME 2023 42nd International Conference on Ocean, Offshore and Arctic Engineering, 11th–16th June, Melbourne.
Chaplin, J., 1996. On frequency-focusing unidirectional waves. Int. J. Offshore Polar Eng. 6, 131–137.
Chen, L.F., Zang, J., Taylor, P.H., Sun, L., Morgan, G.C.J., Grice, J., Orszaghova, J., Tello Ruiz, M., 2018. An experimental decomposition of nonlinear forces on a surface-piercing column: stokes-type expansions of the force harmonics. J. Fluid Mech. 848, 42–77.
Chow, A.D., Rogers, B.D., Lind, S.J., Stansby, P.K., 2019. Numerical wave basin using incompressible smoothed particle hydrodynamics (ISPH) on a single GPU with vertical cylinder test cases. Comput. Fluids 179, 543–562.
Dalrymple, R.A., Rogers, B.D., 2006. Numerical modeling of water waves with the SPH method. Coast. Eng. 53, 141–147.
De Padova, D., Ben Meftah, M., De Serio, F., Mossa, M., Sibilla, S., 2020. Characteristics of breaking vorticity in spilling and plunging waves investigated numerically by SPH. Environ. Fluid Mech. 20, 233–260.
Domínguez, J.M., Altomare, C., Gonzalez-Cao, J., Lomonaco, P., 2019. Towards a more complete tool for coastal engineering: solitary wave generation, propagation and breaking in an SPH-based model. Coast. Eng. J. 61, 15–40.
Domínguez, J.M., Fourtakas, G., Altomare, C., Canelas, R.B., Tafuni, A., García-Feal, O., Martínez-Estévez, I., Mokos, A., Vacondio, R., Crespo, A.J.C., Rogers, B.D., Stansby, P.K., Gómez-Gesteira, M., 2022. DualSPHysics: from fluid dynamics to multiphysics problems. Comput. Part. Mech. 9, 867–895.
Draycott, S., Nambiar, A., Sellar, B., Davey, T., Venugopal, V., 2019. Assessing extreme loads on a tidal turbine using focused wave groups in energetic currents. Renew. Energy 135, 1013–1024.
El Rahi, J., Martínez-Estévez, I., Tagliafierro, B., Domínguez, J.M., Crespo, A.J.C., Stratigaki, V., Suzuki, T., Troch, P., 2023. Numerical investigation of wave-induced flexible vegetation dynamics in 3D using a coupling between DualSPHysics and the FEA module of Project Chrono. Ocean Eng. 285, 115227.
English, A., Domínguez, J.M., Vacondio, R., Crespo, A.J.C., Stansby, P.K., Lind, S.J., Chiapponi, L., Gómez-Gesteira, M., 2022. Modified dynamic boundary conditions (mDBC) for general-purpose smoothed particle hydrodynamics (SPH): application to tank sloshing, dam break and fish pass problems. Comput. Part. Mech. 9, 1–15.
Esandi, J.M., Buldakov, E., Simons, R., Stagonas, D., 2020. An experimental study on wave forces on a vertical cylinder due to spilling breaking and near-breaking wave groups. Coast. Eng. 162, 103778.
Faltinsen, O.M., 1993. Sea Loads on Ships and Offshore Structures. Cambridge University Press.
Fernández, H., Sriram, V., Schimmels, S., Oumeraci, H., 2014. Extreme wave generation using self correcting method—revisited. Coast. Eng. 93, 15–31.
Fourtakas, G., Dominguez, J.M., Vacondio, R., Rogers, B.D., 2019. Local uniform stencil (LUST) boundary condition for arbitrary 3-D boundaries in parallel smoothed particle hydrodynamics (SPH) models. Comput. Fluids 190, 346–361.
Gao, Y., Zhu, J., Wang, L., Li, W., 2023. Experimental investigation of breaking regular waves slamming on offshore wind jacket structure. Ocean Eng. 279, 114528.
Gingold, R.A., Monaghan, J.J., 1977. Smoothed particle hydrodynamics: theory and application to non-spherical stars. Mon. Not. R. Astron. Soc. 181, 375–389.
Gómez-Gesteira, M., Rogers, B.D., Dalrymple, R.A., Crespo, A.J.C., 2010. State-of-the-art of classical SPH for free-surface flows. J. Hydraul. Res. 48, 6–27.
Gotoh, H., Khayyer, A., 2016. Current achievements and future perspectives for projection-based particle methods with applications in ocean engineering. J. Ocean Eng. Mar. Energy 2, 251–278.
Hughes, J.P., Graham, D.I., 2010. Comparison of incompressible and weakly-compressible SPH models for free-surface water flows. J. Hydraul. Res. 48, 105–117.
Issa, R., Violeau, D., 2009. Modelling a plunging breaking solitary wave with eddy-viscosity turbulent SPH models. Comput. Mater. Continua 8, 151–164.
Ji, X., Liu, S., Li, J., Jia, W., 2015. Experimental investigation of the interaction of multidirectional irregular waves with a large cylinder. Ocean Eng. 93, 64–73.
Khayyer, A., Gotoh, H., Shao, S.D., 2008. Corrected Incompressible SPH method for accurate water-surface tracking in breaking waves. Coast. Eng. 55, 236–250.
Khayyer, A., Gotoh, H., Falahaty, H., Shimizu, Y., 2018. An enhanced ISPH-SPH coupled method for simulation of incompressible fluid-elastic structure interactions. Comput. Phys. Commun. 232, 139–164.
Khayyer, A., Shimizu, Y., Gotoh, H., Hattori, S., 2021. Multi-resolution ISPH-SPH for accurate and efficient simulation of hydroelastic fluid-structure interactions in ocean engineering. Ocean Eng. 226, 108652.
Khayyer, A., Shimizu, Y., Gotoh, T., Gotoh, H., 2023. Enhanced resolution of the continuity equation in explicit weakly compressible SPH simulations of incompressible free-surface fluid flows. Appl. Math. Model. 116, 84–121.
Lee, E.-S., Moulinec, C., Xu, R., Violeau, D., Laurence, D., Stansby, P., 2008. Comparisons of weakly compressible and truly incompressible algorithms for the SPH mesh free particle method. J. Comput. Phys. 227, 8417–8436.
Leimkuhler, B., Matthews, C., 2015. Introduction. Molecular dynamics: With Deterministic and Stochastic Numerical Methods. Springer, Switzerland, pp. 1–51.
Li, J., Zhang, H., Liu, S., Fan, Y., Zang, J., 2022. Experimental investigations of secondary load cycle formation in wave force on a circular cylinder under steep regular waves. Ocean Eng. 253, 111265.
Lind, S.J., Stansby, P.K., Rogers, B.D., 2016. Fixed and moored bodies in steep and breaking waves using SPH with the Froude–Krylov approximation. J. Ocean Eng. Mar. Energy 2, 331–354.
Liu, M.B., Liu, G.R., 2010. Smoothed Particle Hydrodynamics (SPH): an overview and recent developments. Arch. Comput. Methods Eng. 17, 25–76.
Lucy, L.B., 1977. A numerical approach to the testing of the fission hypothesis. Astron. J. 82, 1013–1024.
Luo, M., Khayyer, A., Lin, P., 2021. Particle methods in ocean and coastal engineering. Appl. Ocean Res. 114, 102734.
Makris, C.V., Memos, C.D., Krestenitis, Y.N., 2016. Numerical modeling of surf zone dynamics under weakly plunging breakers with SPH method. Ocean Model. 98, 12–35.
Martínez-Estévez, I., Domínguez, J.M., Tagliafierro, B., Canelas, R.B., García-Feal, O., Crespo, A.J.C., Gómez-Gesteira, M., 2023. Coupling of an SPH-based solver with a multiphysics library. Comput. Phys. Commun. 283, 108581.
Monaghan, J.J., 1992. Smoothed particle hydrodynamics. Annu. Rev. Astron. Astrophys. 30, 543–574.
Monaghan, J.J., 1994. Simulating free surface flows with SPH. J. Comput. Phys. 110, 399–406.
Morison, J.R., O'Brien, M.P., Johnson, J.W., Schaaf, S.A., 1950. The force exerted by surface waves on piles. J. Pet. Technol. 2, 149–154.
Ni, X., Feng, W., Huang, S., Zhang, Y., Feng, X., 2018. A SPH numerical wave flume with non-reflective open boundary conditions. Ocean Eng. 163, 483–501.
O'Connor, J., Rogers, B.D., 2021. A fluid–structure interaction model for free-surface flows and flexible structures using smoothed particle hydrodynamics on a GPU. J. Fluids Struct. 104, 103312.
Rapp, R.J., Melville, W.K., 1990. Laboratory measurements of deep-water breaking waves. Philos. Trans. Roy. Soc. Lond. A Math. Phys. Eng. Sci. 331, 735–800.
Schmittner, C., Kosleck, S., Hennig, J., 2009. A phase-amplitude iteration scheme for the optimization of deterministic wave sequences. In: Proceedings of the ASME 28th International Conference on Ocean, Offshore and Arctic Engineering, 31st May–5th June, Honolulu.
Shadloo, M.S., Oger, G., Le Touzé, D., 2016. Smoothed particle hydrodynamics method for fluid flows, towards industrial applications: motivations, current state, and challenges. Comput. Fluids 136, 11–34.
Shao, S., 2006. Simulation of breaking wave by SPH method coupled with k-ϵ model. J. Hydraul. Res. 44, 338–349.

Shao, S., Lo, E.Y.M., 2003. Incompressible SPH method for simulating Newtonian and non-Newtonian flows with a free surface. Adv. Water Resour. 26, 787–800.
Subbulakshmi, A., Verma, M., Keerthana, M., Sasmal, S., Harikrishna, P., Kapuria, S., 2022. Recent advances in experimental and numerical methods for dynamic analysis of floating offshore wind turbines—an integrated review. Renew. Sustain. Energy Rev. 164, 112525.
Suja-Thauvin, L., Krokstad, J.R., Bachynski, E.E., de Ridder, E.-J., 2017. Experimental results of a multimode monopile offshore wind turbine support structure subjected to steep and breaking irregular waves. Ocean Eng. 146, 339–351.
Sun, P., Ming, F., Zhang, A., 2015. Numerical simulation of interactions between free surface and rigid body using a robust SPH method. Ocean Eng. 98, 32–49.
Sun, P.N., Le Touzé, D., Zhang, A.M., 2019. Study of a complex fluid-structure dam-breaking benchmark problem using a multi-phase SPH method with APR. Eng. Anal. Bound. Elem. 104, 240–258.
Sun, P.N., Le Touzé, D., Oger, G., Zhang, A.M., 2021. An accurate FSI-SPH modeling of challenging fluid-structure interaction problems in two and three dimensions. Ocean Eng. 221, 108552.
Sun, P.N., Pilloton, C., Antuono, M., Colagrossi, A., 2023. Inclusion of an acoustic damper term in weakly-compressible SPH models. J. Comput. Phys. 483, 112056.
Tafuni, A., Domínguez, J.M., Vacondio, R., Crespo, A.J.C., 2018. A versatile algorithm for the treatment of open boundary conditions in Smoothed particle hydrodynamics GPU models. Comput. Methods Appl. Mech. Engrg. 342, 604–624.
Tagliafierro, B., Martínez-Estévez, I., Domínguez, J.M., Crespo, A.J.C., Göteman, M., Engström, J., Gómez-Gesteira, M., 2022. A numerical study of a taut-moored point-absorber wave energy converter with a linear power take-off system under extreme wave conditions. Appl. Energy 311, 118629.
Tagliafierro, B., Karimirad, M., Altomare, C., Göteman, M., Martínez-Estévez, I., Capasso, S., Domínguez, J.M., Viccione, G., Gómez-Gesteira, M., Crespo, A.J.C., 2023. Numerical validations and investigation of a semi-submersible floating offshore wind turbine platform interacting with ocean waves using an SPH framework. Appl. Ocean Res. 141, 103757.
Tan, Z., Sun, P.-N., Liu, N.-N., Li, Z., Lyu, H.-G., Zhu, R.-H., 2023. SPH simulation and experimental validation of the dynamic response of floating offshore wind turbines in waves. Renew. Energy 205, 393–409.
Tasora, A., Serban, R., Mazhar, H., Pazouki, A., Melanz, D., Fleischmann, J., Taylor, M., Sugiyama, H., Negrut, D., 2016. Chrono: an open source multi-physics dynamics engine. Lecture Notes in Computer Science. Springer International Publishing, pp. 19–49.
Verbrugghe, T., Domínguez, J.M., Altomare, C., Tafuni, A., Vacondio, R., Troch, P., Kortenhaus, A., 2019. Non-linear wave generation and absorption using open boundaries within DualSPHysics. Comput. Phys. Commun. 240, 46–59.
Violeau, D., Rogers, B.D., 2016. Smoothed particle hydrodynamics (SPH) for free-surface flows: past, present and future. J. Hydraul. Res. 54, 1–26.
Wang, S., Larsen, T.J., Bredmose, H., 2020. Experimental and numerical investigation of a jacket structure subject to steep and breaking regular waves. Mar. Struct. 72, 102744.
Wang, Z.-B., Chen, R., Wang, H., Liao, Q., Zhu, X., Li, S.-Z., 2016. An overview of smoothed particle hydrodynamics for simulating multiphase flow. Appl. Math. Model. 40, 9625–9655.
Wen, H., Ren, B., Dong, P., Wang, Y., 2016. A SPH numerical wave basin for modeling wave-structure interactions. Appl. Ocean Res. 59, 366–377.
Wendland, H., 1995. Piecewise polynomial, positive definite and compactly supported radial functions of minimal degree. Adv. Comput. Math. 4, 389–396.
Yang, Y., Draycott, S., Stansby, P.K., Rogers, B.D., 2023a. A numerical flume for waves on variable sheared currents using smoothed particle hydrodynamics (SPH) with open boundaries. Appl. Ocean Res. 135, 103527.
Yang, Y., Stansby, P.K., Rogers, B.D., Buldakov, E., Stagonas, D., Draycott, S., 2023b. The loading on a vertical cylinder in steep and breaking waves on sheared currents using smoothed particle hydrodynamics. Phys. Fluids 35, 087132.
Ye, T., Pan, D., Huang, C., Liu, M., 2019. Smoothed particle hydrodynamics (SPH) for complex fluid flows: recent developments in methodology and applications. Phys. Fluids 31, 011301.
Zang, J., Taylor, P.H., Morgan, G., Stringer, R., Orszaghova, J., Grice, J., Tello, M., 2010. Steep wave and breaking wave impact on offshore wind turbine foundations—ringing re-visited. In: Proceedings of the 25th International Workshop on Water Waves and Floating Bodies, 9th–12th May, Harbin.
Zhang, F., Crespo, A.J.C., Altomare, C., Domínguez, J.M., Marzeddu, A., Shang, S., Gómez-Gesteira, M., 2018. DualSPHysics: a numerical tool to simulate real breakwaters. J. Hydrodyn. 30, 95–105.
Zhu, J., Gao, Y., Wang, L., Li, W., 2022. Experimental investigation of breaking regular and irregular waves slamming on an offshore monopile wind turbine. Mar. Struct. 86, 103270.